IEEE Photonics Journal
An IEEE Photonics Society Publication

Open Access

Silicon Nitride based Medium Contrast Gratings for Doubly Resonant Fluorescence Enhancement

Volume 11, Number 4, August 2019

Sruti Hemachandran Geetha Menon
Lal Krishna A. S.
Varun Raghunathan

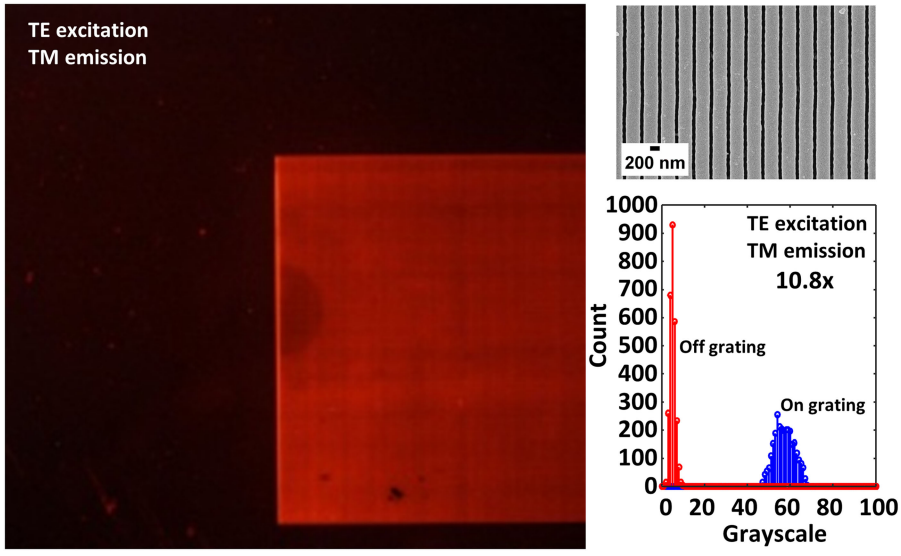

DOI: 10.1109/JPHOT.2019.2909794
1943-0655 © 2019 IEEE

IEEE photonics SOCIETY

IEEE

Silicon Nitride based Medium Contrast Gratings for Doubly Resonant Fluorescence Enhancement

Sruti Hemachandran Geetha Menon, Lal Krishna A. S., and Varun Raghunathan

Department of Electrical and Communication Engineering, Indian Institute of Science, Bengaluru 560012, India

DOI:10.1109/JPHOT.2019.2909794
1943-0655 © 2019 IEEE. Translations and content mining are permitted for academic research only. Personal use is also permitted, but republication/redistribution requires IEEE permission. See http://www.ieee.org/publications_standards/publications/rights/index.html for more information.

Manuscript received January 28, 2019; revised March 23, 2019; accepted April 2, 2019. Date of publication April 9, 2019; date of current version June 27, 2019. This work was supported by Indian Space Research Organization (ISRO), Department of Science and Technology-Science and Engineering Research board (DST-SERB) and MHRD, MeiTY and DST Nano Mission through NNetRA. Corresponding author: Varun Raghunathan (e-mail: varunr@iisc.ac.in).

Abstract: We present the design, fabrication, and experimental characterization of silicon nitride based medium-index contrast gratings on glass substrate for fluorescence enhancement in the yellow to red spectral range with resonances for both incident excitation and fluorescence emission wavelengths under surface normal incidence. A comparison of the design space to realize resonant field enhancement in high-index contrast silicon and medium-index contrast silicon nitride grating structures is presented. The one-dimensional sub-wavelength grating structures studied here are designed with large duty cycle (∼80%) to account for the medium refractive index contrast ($\Delta n \sim 0.5$) between silicon nitride and the glass substrate to ensure that the device operates in the two-mode regime. The resonant enhancement of fluorescence is experimentally verified using rhodamine-B isothiocyanate dye as the fluorophore of interest. A resonant enhancement of 10.8 times is demonstrated in this sample when compared to un-patterned film for transverse electric-transverse magnetic (TE–TM) polarization combination. We have also performed simulation study with plane wave excitation and incoherent dipole array emission to model the resonant excitation and emission processes, respectively. The simulations corroborate well with the best observed experimental results for the doubly resonant fluorescence configuration. Silicon nitride based medium contrast gratings are a promising platform to fabricate scalable structures for resonant enhancement of light–matter interaction with potential applications in high-sensitivity biological fluorescence assays and as a platform for polarization selective interrogation of light emission from nanoscale emitters attached to the grating.

Index Terms: Subwavelength gratings, guided-mode resonance, fluorescence, optical resonance.

1. Introduction

Photonic structures that enhance light-matter interaction at the sub-wavelength scale are attractive for high sensitivity optical sensors based on refractive index sensing, light absorption and emission modalities [1]. In particular, fluorescence emission-based sensing at low analyte concentration by making use of optical resonance phenomenon in plasmonic [2]–[4] and dielectric structures [5], [6] has been pursued actively. Such structures find applications in high sensitivity enzyme-linked fluorescence assays (ELFA) for low concentration detection of bio-markers [7]. Large area

photonic crystal structures composed of one-dimensional sub-wavelength patterns of polymers or glass with deposited Titanium dioxide (TiO_2) thin films have been used successfully to create high quality factor guided-mode resonances (GMR) with multifold enhancement in fluorescence [5]. Such structures have also been used to create dual excitation resonances at different incidence angles for multiplexed fluorescence assays [6]. The fluorescence assays with polymer layers are inherently limited by the fluorescence exhibited by the polymer material. The use of sputtered TiO_2 layers on patterned quartz substrates minimizes the background fluorescence, however the limited technology to deposit thick layers of optical quality TiO_2 or etch TiO_2 structures with good quality sidewalls limits the design space of such GMR structures.

Silicon based sub-wavelength grating structures comprising of fully etched high index gratings on low-index substrates, called high-contrast gratings (HCGs) have been used to create robust resonant devices for applications such as laser end-mirrors, broad-band filter and as refractive index sensors [8]. Such resonant structures operate in the so-called dual-mode sub-wavelength grating region leading to intricate resonant features due to the mutual interference and interaction of the oscillating super-modes at the grating interfaces [8]. However, silicon based resonant structures exhibit low efficiency for fluorescence sensing applications owing to the large absorption coefficient of silicon in the visible region. Silicon nitride on the other hand offers an alternate platform with medium refractive index contrast with respect to glass substrates, low absorption window in the visible region and can also be fabricated into sub-wavelength grating structures with characteristic resonance properties. Silicon nitride sub-wavelength grating structures have been used previously for guided-mode resonance filters [9], refractive index sensing [10] and resonant enhancement of nonlinear harmonic generation [11]. Inherent photoluminescence from silicon nitride films has also been minimized by optimizing the thin-film deposition and annealing process [12]. Such structures being compatible with silicon fabrication are also amenable to large scale fabrication using standard silicon processing techniques.

In this paper, we report the design, fabrication and experimental characterization of silicon nitride sub-wavelength gratings on glass substrates (termed as medium-contrast gratings or MCGs) and demonstrate its applications for resonant enhancement of fluorescence in the yellow-to-red spectral region. To achieve a prominent dual-mode interaction region in such structures, gratings were designed with an increased duty cycle leading to higher effective refractive index for the gratings, resulting in well-defined resonant features. The structures designed here are polarization-dependent due to its 1D periodicity [8] and are doubly-resonant for excitation at transverse electric (TE) polarization and emission at transverse magnetic (TM) polarization. Throughout the paper, the electric field directions parallel and perpendicular to the gratings are termed as TE and TM polarizations respectively. The enhancement of fluorescence was ascertained by functionalizing the surface with Rhodamine-B isothiocyanate (RITC), with maximum fluorescence enhancement of 10.8 obtained experimentally for excitation and emission at TE and TM polarization respectively, when compared to un-patterned thin films functionalized with the fluorophores. The enhancement obtained is further simulated by modelling the fluorescence process using incoherent summation of dipole emitters taking into account the effect of the grating structure in enhancing both the excitation and emission resonant fields. Doubly resonant fluorescence structures as discussed here can find potential applications in high-sensitivity fluorescence assays for biological applications [7] and for studying polarization-selective nano-scale emitter-structure interaction, for example in low-dimensional materials, such as emerging two-dimensional layered materials [13].

2. Design of Silicon Nitride MCG for Fluorescence Applications

It is instructive to compare the performance of sub-wavelength gratings comprising of high-index contrast silicon with the medium-index contrast silicon nitride structures on glass substrates to understand the design space as a function of the refractive index contrast. A schematic of the one-dimensional, fully-etched sub-wavelength gratings studied here is shown in Fig. 1(a) with the TE and TM polarization directions for normal incidence excitation. The transmission contour for 50% duty cycle ((Λ-a)/Λ = 0.5) silicon HCGs and silicon nitride MCGs on

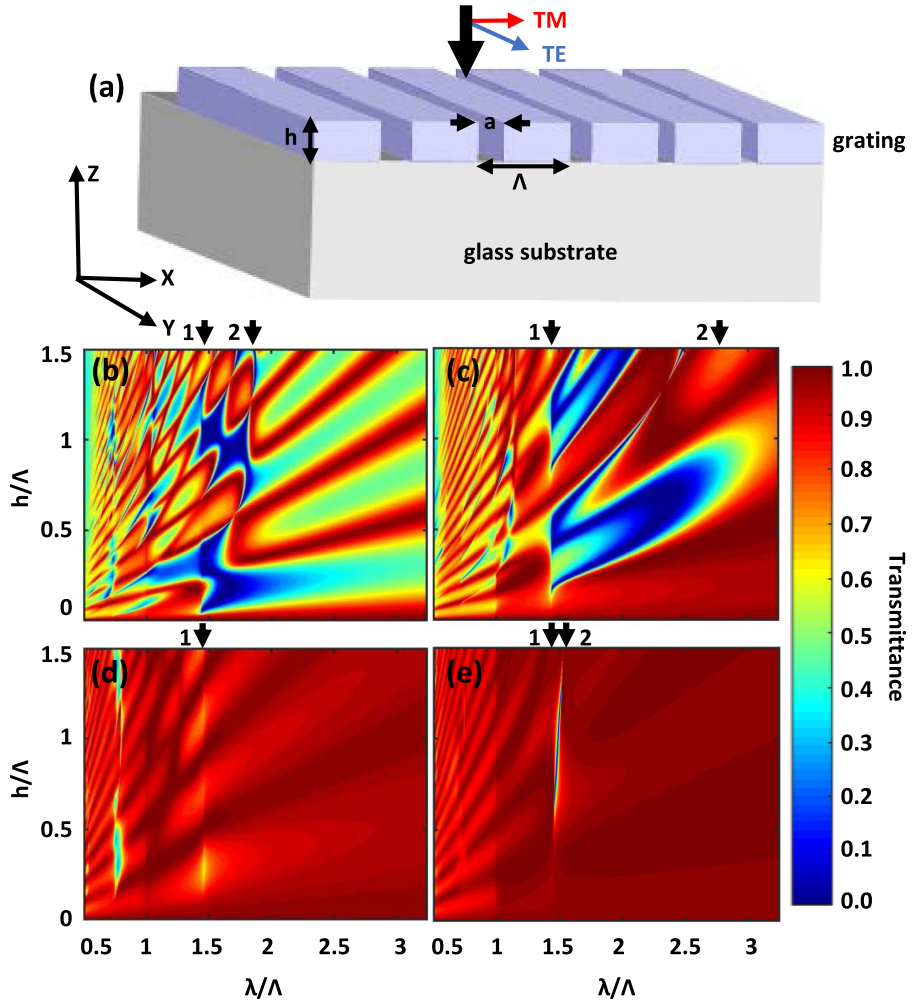

Fig. 1. (a) Schematic of sub-wavelength grating structures showing the co-ordinate axes, incident light direction and polarization directions. Simulated transmission contours for 50% duty cycle (b–c) silicon HCGs and (d–e) silicon nitride MCGs. Incident polarizations considered are: (b–d) TE polarized and (c–e) TM polarized. Arrows 1 and 2 mark the dual mode region spanning between higher order diffraction and deep sub-wavelength regions respectively.

glass substrate simulated using Rigorous coupled-wave analysis (RCWA) simulation tool, S4 [14] is illustrated in Fig. 1(b)–(e) as a function of the normalized wavelength and normalized structure height (normalized by the grating period). The dual-mode region spans the spectral region shown by arrows 1 and 2 in the figure with arrow 1 denoting the transition from sub-wavelength grating regime to higher order diffraction regime and arrow 2 denoting the transition from sub-wavelength grating regime to deep sub-wavelength regime, in which the gratings acts as an effective index medium [8]. Comparing figure 1(b), (c) and (d), (e), it is clear that the spectral window over which the dual-mode region is observed is narrower for the silicon nitride structure when compared to silicon structures due to the medium index contrast between the grating layer and the glass substrate. Increasing the effective refractive index of the grating layer is expected to widen the dual-mode spectral window in the case of silicon nitride structures. This is accomplished by increasing the width of the silicon nitride gratings at the expense of the air-gap for a fixed grating pitch. Similar transmission contour plots have been shown in Ref. [10] for silicon nitride gratings with duty cycle of 70%. Fig. 2 shows a series of transmission spectra for both TE and TM incident polarization with increasing duty-cycle for a fixed normalized thickness of 0.73. The resonance feature shifts to longer wavelengths with

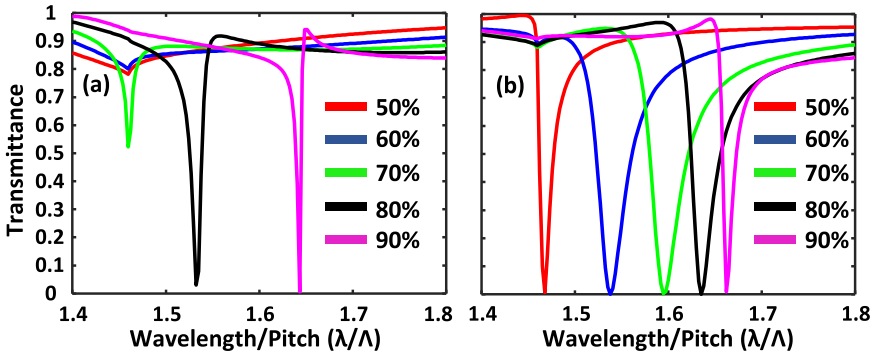

Fig. 2. Transmission spectra of silicon nitride MCGs for varying duty cycles for a normalized thickness of 0.73, for: (a) TE and (b) TM polarization.

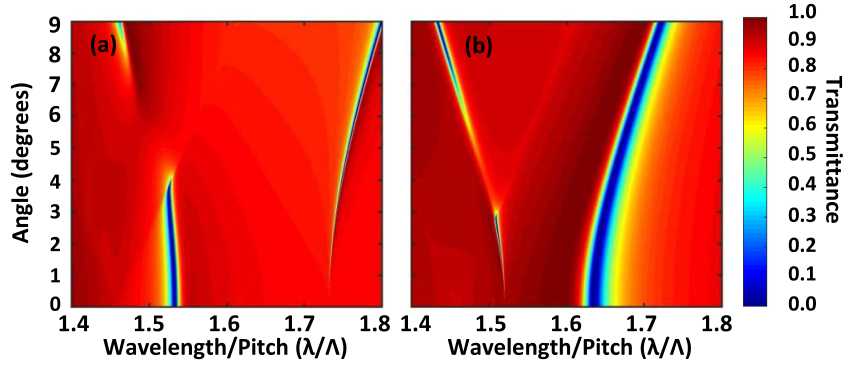

Fig. 3. Angle dependence of the transmission spectra for: (a) TE and (b) TM polarization.

increased contrast as the duty cycle is increased. This strategy is however limited by the critical dimension, i.e., the airgap achievable by the lithography techniques. Patterning using electron beam lithography restricts the minimum feature size to 20–50 nm depending on the type and thickness of e-beam resist, e-beam lithography operating voltage, time of patterning and the development conditions [15].

The angular dependence of the resonance is important as the excitation/ emission intensities are considered over certain angular range as determined by the numerical aperture (NA) of the objective lens, and this influences the observed resonance enhancement. To study the angle dependence of the grating resonances, Fig. 3(a) and (b) shows the transmission spectra for TE and TM mode resonances obtained for varying angles of incidence for a fixed normalized thickness of 0.73 and duty cycle of 80%. At normal incidence, prominent resonances are observed at normalized wavelengths of 1.53 and 1.64 for TE and TM polarizations respectively. For increasing incidence angles, new resonance features are observed at longer wavelengths (at $\sim$1.75) for TE resonance, while the normal incidence resonance mode remains prominent accompanied by a red-shift for TM resonance.

The silicon nitride MCG dimensions were designed to overlap the spectral resonances with the fluorescence spectrum of fluorophores in the yellow to red spectral region. The MCG structures were optimized using finite difference time domain (FDTD - Lumerical) simulations. The transmission spectra and excitation/ emission characteristics of RITC, a typical fluorescence dye with a quantum yield of 0.9 [16] used in the experimental study to be described below are shown in Fig. 4(a), (b). Fluorophores with similar fluorescence characteristics, such as TRITC, Alexa 550, and Texas Red, which are routinely used in ELFA arrays can also be enhanced using the same structure.

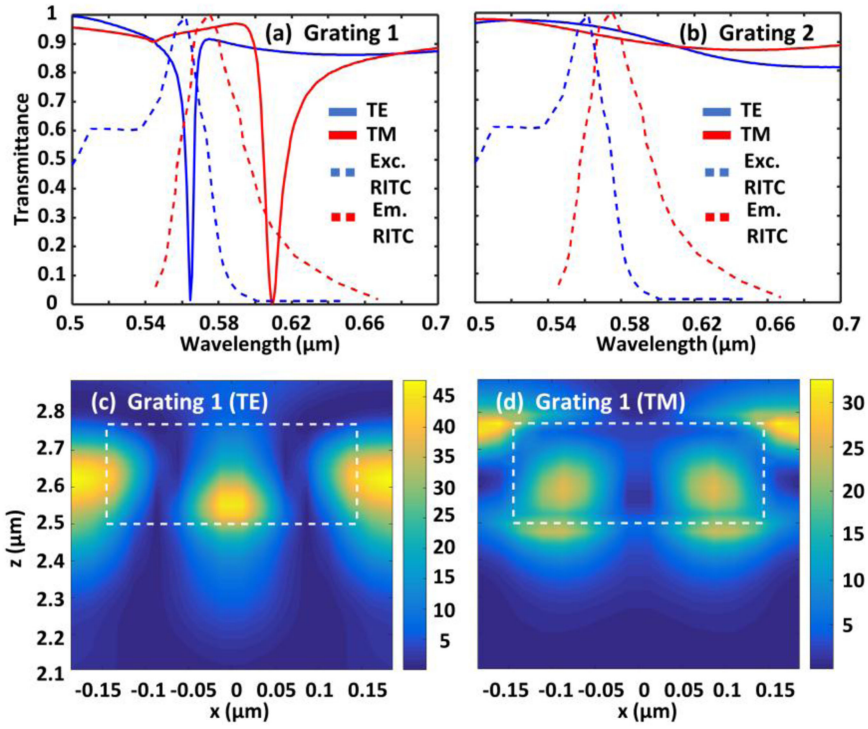

Fig. 4. Simulated transmission spectra of the sub-wavelength gratings: (a) grating-1 with h = 270 nm, Λ = 370 nm and duty cycle = 78%. (b) grating-2 with h = 270 nm, Λ = 500 nm and duty cycle = 84%. The fluorescence excitation/ emission spectrum of RITC are also shown. Electric field intensity profile of the grating on-resonance for (c) TE and (d) TM polarizations.

For the present study, the optimum duty cycle for silicon nitride MCGs has been chosen around 80% considering the presence of dual mode region for both incident polarizations and the feasibility of fabrication of the grating structures. For a fixed silicon nitride film thickness, h = 270 nm, two different grating structures with different pitch, duty cycle combinations are considered, namely: (1) 370 nm, 78% and (2) 500 nm, 84% with the spectral features on- and off-resonance with the fluorescence spectra respectively, as shown in Fig. 4(a), (b). This is to investigate the on- and off-resonance fluorescence enhancement due to the grating structure. Grating-1 is designed to show resonance dips at 564.8 nm and 609.1 nm with Quality factors (Q) of 152 and 52 for TE and TM polarization respectively with good overlap of the RITC spectra. Grating-2 is designed for resonances at longer wavelengths, ~760 nm and 780 nm for TE and TM polarization respectively (not shown here), resulting in off-resonance due to relatively flat spectral feature across the RITC spectra, as shown in Fig. 4(b). The spectral features on-resonance are attributed to crossing-type resonance in the dual-mode region [8]. The field intensity profiles shown in Fig. 4(c), (d) for grating-1 show maximum resonant intensity, $|E|^2$ enhancement of over 45 and 30 times, when compared to the incident light for the TE and TM incident polarizations respectively, with significant field located in the airgap region.

3. Device Fabrication and Experimental Characterization

The silicon nitride gratings were fabricated on a 500 micrometer thick double side polished borosilicate glass substrate using electron beam lithography with a patterned area of 1 $\times$ 1 mm^2. The grating structures can be scaled to larger areas using stepper [17] or interference [18] lithography techniques. 270 nm thick silicon nitride film was deposited using plasma-enhanced deposition technique on the glass and PMMA-C3 resist of ~300 nm was coated on the film. To dissipate

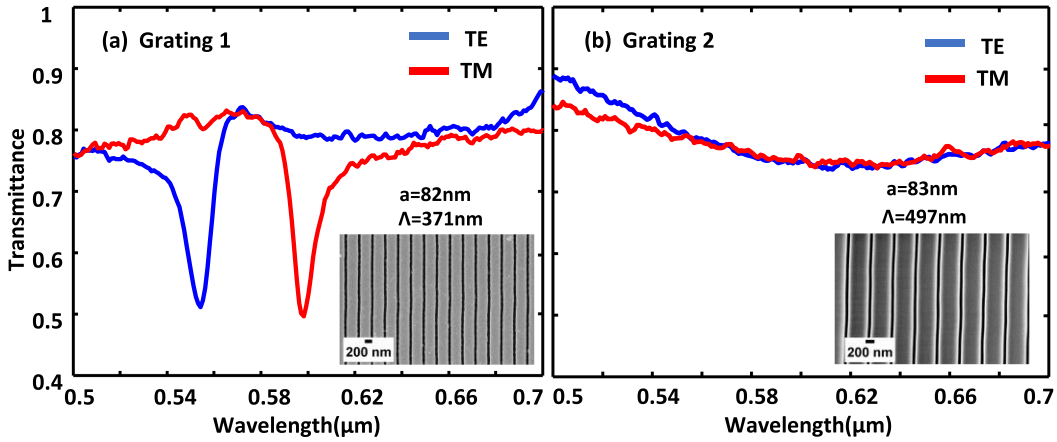

Fig. 5. Experimental transmission spectra of silicon nitride gratings with parameters: (a) $\Lambda = 370$ nm, h = 270 nm, DC = 78%. (b) $\Lambda = 497$ nm, h = 270 nm, DC = 83%. Inset shows SEM image of the corresponding grating structure.

the charges during the writing process, 10 nm aluminum layer was deposited using electron-beam evaporation, which was removed prior to the development of the resist. The underlying silicon nitride was subsequently etched with PMMA-C3 as a mask using reactive ion etching. Two different grating structures as described above were fabricated for on- and off-resonance enhancement study. The top view scanning electron microscopy (SEM) image of the fabricated gratings is shown in the inset of Fig. 5. The mean dimensions of grating 1 and 2 as obtained using SEM are a = 82 nm, Λ = 371 nm (duty cycle = 78%) and a = 83 nm, Λ = 497 nm (duty cycle = 83%) respectively, showing good agreement with the intended design. To functionalize the grating surface with RITC, the gratings were first cleaned with piranha for 10 minutes, silanized and then functionalized with RITC [19], [20]. The silanization was done by immersing the sample in 1%(v/v) 3-Aminopropyl tri-ethoxysilane (APTES) in ethanol solution for 3 hours. After multiple ethanol washes, the sample was incubated in a solution containing 20 μL of triethylamine and 3 mg of RITC in 8 mL of acetonitrile overnight. After multiple washes with acetonitrile and ethanol to remove unattached fluorophore, the sample was blow dried using nitrogen.

The transmission spectra of the fabricated gratings were measured prior to fluorophore functionalization using an UV-Vis spectrometer in the wavelength range of 500 to 700 nm, as shown in Fig. 5, with a polarizer placed before the sample to select the incident polarizations and a circular aperture to restrict the beam size to 1 mm diameter in order to match the beam size to the grating area. The spectra show prominent resonance dips at 554 nm and 598 nm for TE and TM polarization respectively for grating-1 in Fig. 5(a) overlapping well with the RITC spectra. In contrast, grating-2 does not show any resonance feature in this spectral range of interest as shown in Fig. 5(b). The slight discrepancy between the simulated and measured resonance positions can be attributed to variations in the actual and simulated device dimensions. The Q-factor extracted from the resonance feature are 45 and 49 for TE and TM polarizations respectively.

To characterize the enhancement of the fluorescence, fluorescent images of the sample were taken using a standard upright BX-51M fluorescence microscope [21] with lamp illumination with excitation spectral range of 515$-$550 nm and emission filter range set using a long-pass filter with transmission in the range of 590–650 nm. The microscope operates in the reflection mode in which the incident light is focused onto the sample by means of a dichroic mirror and low numerical aperture objective and the emitted light is imaged by a camera through the same objective. The fluorescence excitation and emission were done using 5x/0.15NA objective lens, with the aperture-stop in the excitation path partially closed to allow close to normal incidence excitation and fluorescence emission collected over the full acceptance angle of the lens (0–9°). Images were taken with two separate polarizers in the excitation and emission path of the microscope, with the background

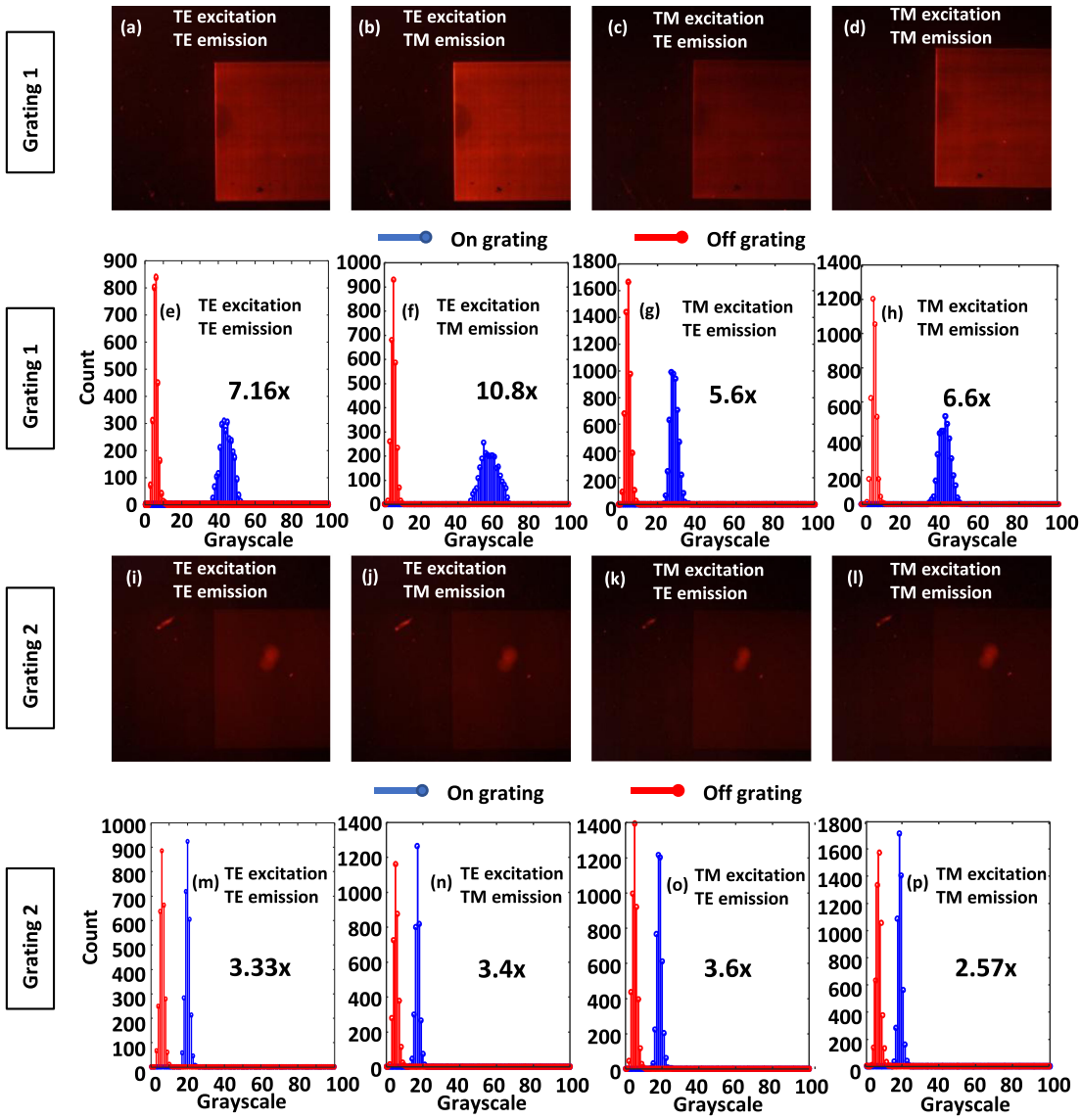

Fig. 6. Polarization dependent fluorescence images of: (a–d) grating 1and (i–l) grating 2 coated with RITC dye and the corresponding histograms: (e–h) for grating 1 and (m–p) for grating 2.

images subtracted using a reference silicon nitride thin-film on silicon substrate without the fluorophores. The photoluminescence signal from the bare silicon nitride film was below the detection level of the imaging camera. The fluorescent images and the corresponding intensity histograms for the two gratings are shown in Fig. 6. Grating-1 enhances fluorescence more than the grating-2 due to the resonance characteristic that overlaps well with the excitation and emission spectra of RITC. The fluorescence enhancement, defined as the ratio of on-grating to off-grating fluorescence intensity is obtained as ∼10.8 times for TE-TM polarized excitation-emission respectively, consistent with the doubly resonant characteristic of the structure. Lower enhancement is observed for other polarization combinations as listed in the histogram plots of Fig. 6. Unpolarized excitation-emission resulted in meagre enhancement (2.3 times–image not shown here) due to inefficient excitation and emission extraction from the fluorophores [22], while TE-polarized excitation and unpolarized collection resulted in approximately half the enhancement of the TE-TM case (5.8 times–image not shown here). The enhancement was also found to consistently decrease with increasing NA of the

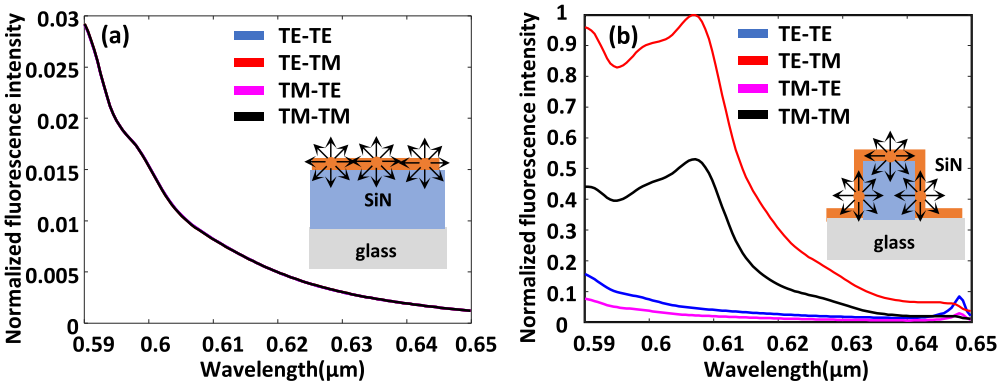

Fig. 7. Calculated normalized fluorescence intensity obtained as an incoherent summation of multiple dipole emitters for: (a) off-grating, un-patterned silicon nitride layer, and (b) on-grating for different excitation-emission polarizations considering excitation and emission filters of 515–580 nm and 590–650 nm respectively. A schematic of the off-and on-grating structure with representative dipoles is shown in the inset of the figure.

objective lens (data not shown here) due to the inclusion of larger excitation/ emission acceptance angles reducing the effect of resonant field enhancement from the grating structures.

4. Discussion

To understand the experimentally observed doubly-resonant fluorescence enhancement from the grating structures, the fluorescence emission from fluorophores attached to the 1D gratings were modelled by incoherent summation of dipole emitters using FDTD based simulations. A schematic of the studied structure is shown in the inset of Fig. 7(a), (b) for the off- and on- grating cases. Plane wave excitation at normal incidence was used to simulate the excitation, representing the experimental excitation with the aperture-stop partially closed. The absorption of the incident light by the fluorophore layer was calculated as the product of field intensity profile on the structure and normalized excitation cross-section of the fluorophore integrated over the excitation wavelengths of interest, given by:

$$I_{abs}(x, z) \propto \int_{\lambda ex} \sigma_{ex}(\lambda_{ex}) |E_{ex}(\lambda_{ex}, x, z)|^2 d\lambda \tag{1}$$

where σ_{ex} is the normalized excitation cross section, shown in Fig. 4, blue dashed curve and $|E_{ex}|^2$ is the electric field intensity enhancement at particular position (x, z) along the structure, shown in Fig. 4(c).

The fluorescence emission was simulated using discrete dipole emitters placed along the surface of the film or the sidewalls of the grating, as shown in the inset of Fig. 7. The fluorescence dye coating of ~8 nm thickness used in the experimental study (determined using Atomic Force Microscope) was modelled using a total of 47 dipoles distributed across the unit-cell. The maximum number of dipoles to be simulated was verified by a convergence test of the overall fluorescence enhancement with increasing number of dipoles placed across multiple unit cells. For each dipole emitter, the total radiated field intensity collected by the objective lens in the far-field can be represented as:

$$I_{em}(x, z) \propto \int_{\lambda em} \int_{\theta} \sigma_{em}(\lambda) |E_{em}(\lambda, \theta, x, z)|^2 d\theta d\lambda \tag{2}$$

where, σ_{em} is the normalized emission cross section of the dye, shown in Fig. 4, red dashed curve and $|E_{em}|^2$ is the intensity collected due to the radiating dipole at a given location (x, z) over the angle θ extending over the acceptance angle range of the objective lens. The fluorescence emission spectrum was obtained by incoherently summing the individual dipole emission considering all three possible emission dipole orientations (x, y or z oriented), after suitably weighing the emission with

TABLE 1
Comparison of Experimental and Simulated Fluorescence Enhancement for Different Excitation/ Emission Configurations

Polarization configuration (Excitation/ Emission)	**Experiment** λ_{res}=554 nm (TE), 598 nm (TM) Exc. Filter: 515-550 nm Em. Filter: 590-650 nm	**Simulation studies** λ_{res}=564.8 nm (TE), 609.1 nm (TM) Exc. Filter: 515-580 nm Em. Filter: 590-650 nm
TE/TM	10.8	58.6
TE/TE	7.2	5.6
TM/TM	6.6	27.9
TM/TE	5.6	2.6

the spatially dependent absorption strength for each of the dipoles, as calculated in equation (1). The fluorescence spectrum collected using the objective lens is given as:

$$I(\lambda) \propto \sum_{dipoles} \left(\int_{\lambda ex} \sigma_{ex}(\lambda) |E_{ex}(\lambda, x, z)|^2 d\lambda \right) \times \int_{\theta} \sigma_{em}(\lambda) |E_{em}(\lambda, \theta, x, z)|^2 d\theta \tag{3}$$

The structures simulated are the same as that for which resonance spectra and electric field intensity profiles are shown in Fig. 4 with resonances at 564.8 nm and 609.1 nm for TE and TM polarization respectively. Fig. 7(a) and (b) shows the fluorescence spectrum as a function of the emission wavelength, obtained off- and on- grating for four different excitation-emission polarization combinations with the peaks normalized by the maximum value of fluorescence signal (corresponding to the on-grating for TE-TM case). The excitation and emission wavelength range considered for this simulation are 515–580 nm and 590–650 nm respectively, with emission collected using an objective lens with NA = 0.15 (0 to 9 deg acceptance angle). The off-grating, thin-film fluorescence signal is found to be independent of the polarization combinations (all four curves overlap). In contrast, the on-grating fluorescence signal shows strong polarization dependence due to the resonant field enhancement and enhanced extraction of emitted radiation [22] with the fluorescence signal reaching a maximum at the emission resonance of ~609 nm. This spectrally selective enhancement of the dye fluorescence on-grating can be attributed to the Purcell effect [23] and the associated increase in fluorescence emission rate in the presence of the grating resonance. TE emission curves show a peak at ~648 nm due to the long wavelength resonance observed for TE polarization at increasing incidence angles, as shown in Fig. 3. Highest fluorescence signal is obtained for excitation-emission corresponding to TE-TM as expected based on the overlap of the TE and TM resonances with the fluorescence spectrum in Fig. 4. The overall fluorescence enhancement was calculated by taking the ratio of the total on- and off- grating fluorescence integrated across the emission wavelength range are listed in Table 1 below for various polarization combinations and compared with experimental results.

It should be noted that the spectral positions of the resonance features in the simulation and experiments being different results in the filter spectral range used for excitation and emission also being chosen differently, as listed in the respective columns of Table 1. Irrespective of this difference, the general agreement between the simulations and experiments is good with the same order of magnitude enhancement factors. TE-TM polarization combination results in the highest enhancement in both cases. In the experimental work, the upper filter cut-off of the emission filter at ~550 nm overlaps with the TE excitation resonance feature, resulting in lower excitation efficiency and hence a reduced fluorescence enhancement factor than predicted by simulations. Overlapping the filter bandwidth with the resonance to ensure better excitation of the TE resonance is a possible strategy for further increasing the experimental fluorescence enhancement. The experiments however show TE-TE to be the second highest when compared to TM-TM as obtained through simulations. This

is most likely due to the differences in the Q-factors of the resonances in the simulations (TE:152 and TM:52) and experiments (TE:45 and TM:49) with TE showing higher Q value than TM for the simulations and vice versa for the experiments. The Q values being comparable in the experiment result in only 1.5 times higher fluorescence enhancement for TE-TM when compared to TE-TE, whereas simulations show ∼2.1 times higher fluorescence enhancement for TE-TM when compared to TM-TM. Increase in the overall fluorescence enhancement can be achieved by improving the Q-factor of the resonance by improving the etch process to create good quality sidewalls across the narrow air gaps used in the experiments. Further improvement in Q-factor can be achieved by exploring anti-crossing resonances [8] in the medium contrast grating structures, however it requires larger film thickness to fabricate the grating structures. Two-dimensional sub-wavelength grating structures will also result in polarization independent fluorescence enhancement, which will be highly desirable for biological fluorescence assays [24].

5. Conclusion

The design, fabrication and experimental characterization of silicon nitride based medium contrast gratings for resonant enhancement of fluorescence from fluorophores attached to the surface of the gratings is presented. One-dimensional grating structures were designed with the objective of creating dual resonances for the excitation and emission wavelengths for TE and TM polarizations respectively. The fabricated structures exhibited resonances at 554 nm and 598 nm with Q-factors of 45 and 49 for incident TE and TM polarizations respectively. The surface of the gratings was functionalized with RITC dye and maximum fluorescence enhancement of 10.8 times was observed for excitation-collection polarizations of TE-TM. The experimental observations were corroborated with simulation studies modelling fluorescence enhancement, with excitation resonance modelled with plane-wave illumination and fluorescence emission as incoherent summation of dipole emitters. Further enhancement in fluorescence can be achieved by selecting the excitation/ emission filter range to have better overlap with the resonance spectrum of the grating structure and fluorescence spectrum and utilizing anti-crossing type resonances [8] in the MCG structures. Silicon nitride based medium contrast grating is a promising platform to fabricate CMOS-compatible, scalable structures for resonant enhancement of light-matter interaction and can find potential applications in high-sensitivity fluorescence assays. Doubly resonant gratings as discussed here are particularly attractive for nano-optics applications to selectively excite and probe specific polarizations of light interacting with dielectric nanostructures, especially to probe emerging two-dimensional layered materials.

Acknowledgment

The authors would like to thank Dr. B. Pesala, Ameen E, and S. Gupta of CSIR-CEERI, Chennai campus for helpful discussions and for performing spectrofluorometer measurements on silicon nitride and rhodamine-B samples. The authors would also like to thank Dr. Manoj Varma, Dr. Suman Pahal and Dr. Swathi Suran of the Centre for Nano Science and Engineering Department, Indian Institute of Science, for help with polyelectrolyte based surface functionalization and fluorescence microscopy.

References

[1] M. S. Luchansky and R. C. Bailey, "High-Q optical sensors for chemical and biological analysis," *Analytical Chem.*, vol. 84, no. 2, pp. 793–821, 2011.
[2] M. Chekini, R. Filter, J. Bierwagen, A. Cunningham, C. Rockstuhl, and T. Bürgi, "Fluorescence enhancement in large-scale self-assembled gold nanoparticle double arrays," *J. Appl. Phys.*, vol. 118, no. 23, 2015, Art. no. 233107.
[3] Z. Mei and L. Tang, "Surface-plasmon-coupled fluorescence enhancement based on ordered gold nanorod array biochip for ultrasensitive DNA analysis," *Analytical Chem.*, vol. 89, pp. 633–639, 2017.
[4] M. Bauch, K. Toma, M. Toma, Q. Zhang, and J. Dostalek, "Plasmon-enhanced fluorescence biosensors: A review," *Plasmonics*, vol. 9, pp. 781–799, 2013.

[5] A. Pokhriyal, M. Lu, V. Chaudhery, C.-S. Huang, S. Schulz, and B. T. Cunningham, "Photonic crystal enhanced fluorescence using a quartz substrate to reduce limits of detection," *Opt. Exp.*, vol. 18, pp. 24793–24808, 2010.
[6] A. Pokhriyal, M. Lu, C. S. Huang, S. Schulz, and B. T. Cunningham, "Multicolor fluorescence enhancement from a photonics crystal surface," *Appl. Phys. Lett.*, vol. 97, no. 12, pp. 121108–121110, 2010.
[7] B. T. Cunningham and R. C. Zangar, "Photonic crystal enhanced fluorescence for early breast cancer biomarker detection," *J. Biophoton.*, vol. 8/9, pp. 617–628, 2012.
[8] C. J. Chang-Hasnain and W. Yang, "High-contrast gratings for integrated optoelectronics," *Adv. Opt. Photon.*, vol. 4, pp. 379–440, 2012.
[9] M. J. Uddin and R. Magnusson, "Efficient guided-mode-resonant tunable color filters," *IEEE Photon. Technol. Lett.*, vol. 24, no. 17, pp. 1552–1554, Sep. 2012.
[10] A. Shakoor, M. Grande, J. Grant, and D. R. S. Cumming, "One-dimensional silicon nitride grating refractive index sensor suitable for integration with CMOS detectors," *IEEE Photon. J.*, vol. 9, no. 1, Feb. 2017, Art. no. 6800711.
[11] T. Ning *et al.*, "Efficient second-harmonic generation in silicon nitride resonant waveguide gratings," *Opt. Lett.*, vol. 37, pp. 4269–4271, 2012.
[12] H. Kato, A. Masuzawa, T. Noma, K. S. Seol, and Y. Ohki, "Thermally induced photoluminescence quenching centre in hydrogenated amorphous silicon oxynitride," *J. Phys.: Condens. Matter*, vol. 13, pp. 6541–6549, 2001.
[13] Z. Wang *et al.*, "Giant photoluminescence enhancement in tungsten-diselenide–gold plasmonic hybrid structures," *Nature Commun.*, vol. 7, 2016, Art. no. 11283.
[14] V. Liu and S. Fan, "S4: A free electromagnetic solver for layered periodic structures," *Comput. Phys. Commun.*, vol. 183, pp. 2233–2244, 2012.
[15] A. N. Broers, A. C. F. Hoole, and J. M. Ryan, "Electron beam lithography - Resolution limits," *Microelectron. Eng.*, vol. 32, pp. 131–142, 1996.
[16] L. Jin, Y. Fang, P. Hu, Y. Zhai, E. Wang, and S. Dong, "Polyoxometalate-based inorganic-organic hybrid film structure with reversible electroswitchable fluorescence property," *Chem. Commun.*, vol. 48, no. 15, pp. 2101–2103, 2012.
[17] T. Sun, S. Kan, G. Marriott, and C. J. Chang-Hasnain, "High-contrast grating resonators for label-free detection of disease biomarkers," *Sci. Rep.*, vol. 6, 2016, Art. no. 27482.
[18] S. Behera and J. Joseph, "Design and realization of functional metamaterial basis structures through optical phase manipulation based interference lithography," *J. Opt.*, vol. 19, no. 10, 2017, Art. no. 105103.
[19] P. Saengdee *et al.*, "Surface modification of silicon dioxide, silicon nitride and titanium oxynitride for lactate dehydrogenase immobilization," *Biosensors Bioelectron.*, vol. 67, pp. 134–138, 2015.
[20] T. D. To, A. T. Nguyen, K. N. T. Phan, A. T. T. Truong, T. C. D. Doan, and C. N. Dang, "Modification of silicon nitride surfaces with GOPES and APTES for antibody immobilization: Computational and experimental studies," *Adv. Nat. Sci., Nanosci. Nanotechnol.*, vol. 6, no. 4, 2015, Art. no. 045006.
[21] W. K. Fester, M. Abramowitz, and M. W. Davidson, "Olympus B X 51 fluorescence microscope cutaway diagram." Accessed: Mar. 20, 2019. [Online]. Available: https://www.olympus-lifescience.com/en/microscope-resource/primer/techniques/fluorescence/bx51fluorescence/
[22] N. Ganesh *et al.*, "Leaky-mode assisted fluorescence extraction: Application to fluorescence enhancement biosensors," *Opt. Exp.*, vol. 16, no. 26, pp. 21626–21640, 2008.
[23] E. M. Purcell, "Spontaneous emission probabilities at radio frequencies," *Phys. Rev. Lett.*, vol. 69, 1946, Art. no. 681.
[24] M. Shokooh-Saremi and R. Magnusson, "Properties of two-dimensional resonant reflectors with zero-contrast gratings," *Opt. Lett.*, vol. 39, no. 24, pp. 6958–6961, 2014.